










ARTICLE



<https://doi.org/10.1038/s41467-020-15934-1>

OPEN

# Synthesis of high-entropy alloy nanoparticles on supports by the fast moving bed pyrolysis

Shaojie Gao <sup>1</sup>, Shaoyun Hao <sup>1</sup>, Zhennan Huang <sup>2</sup>, Yifei Yuan <sup>2,3</sup>, Song Han <sup>4</sup>, Lecheng Lei <sup>1,5</sup>,  
Xingwang Zhang <sup>1,5</sup>✉, Reza Shahbazian-Yassar <sup>2</sup> & Jun Lu <sup>3</sup>✉

<sup>1</sup>Key Laboratory of Biomass Chemical Engineering of Ministry of Education, College of Chemical and Biological Engineering, Zhejiang University, 310027 Hangzhou, Zhejiang Province, China. <sup>2</sup>Department of Mechanical and Industrial Engineering, University of Illinois at Chicago, Chicago, IL 60607, USA. <sup>3</sup>Chemical Sciences and Engineering Division, Argonne National Laboratory, 9700 S. Cass Avenue, Lemont, IL 60439, USA. <sup>4</sup>School of Environment and Safety Engineering, Jiangsu University, 212013 Zhenjiang, Jiangsu Province, China. <sup>5</sup>Institute of Zhejiang University-Quzhou, 78 Jinhua Boulevard North, 324000 Quzhou, China. ✉email: [xwzhang@zju.edu.cn](mailto:xwzhang@zju.edu.cn); [junlu@anl.gov](mailto:junlu@anl.gov)

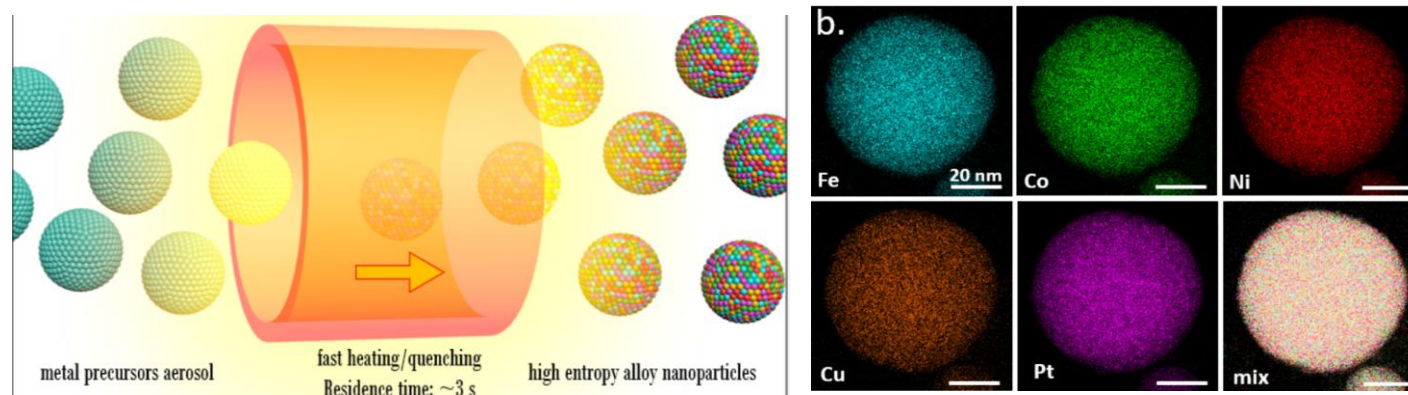
# Multimetallic High-Index Faceted Heterostructured Nanoparticles

Liliang Huang, Haixin Lin, Cindy Y. Zheng, Edward J. Kluender, Rustin Golnabi, Bo Shen, and Chad A. Mirkin\*

*J. Am. Chem. Soc.* 2020, 142, 10, 4570–4575

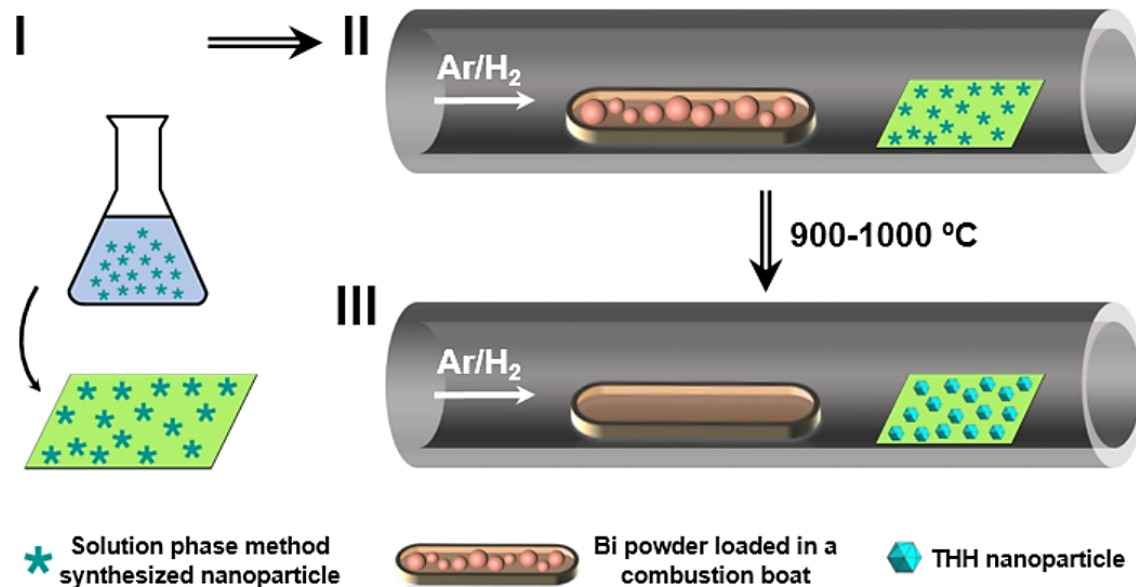
# Aerosol Synthesis of High Entropy Alloy Nanoparticles

Yong Yang, Boao Song, Xiang Ke, Feiyu Xu, Krassimir N. Bozhilov, Liangbing Hu, Reza Shahbazian-Yassar,\* and Michael R. Zachariah\*



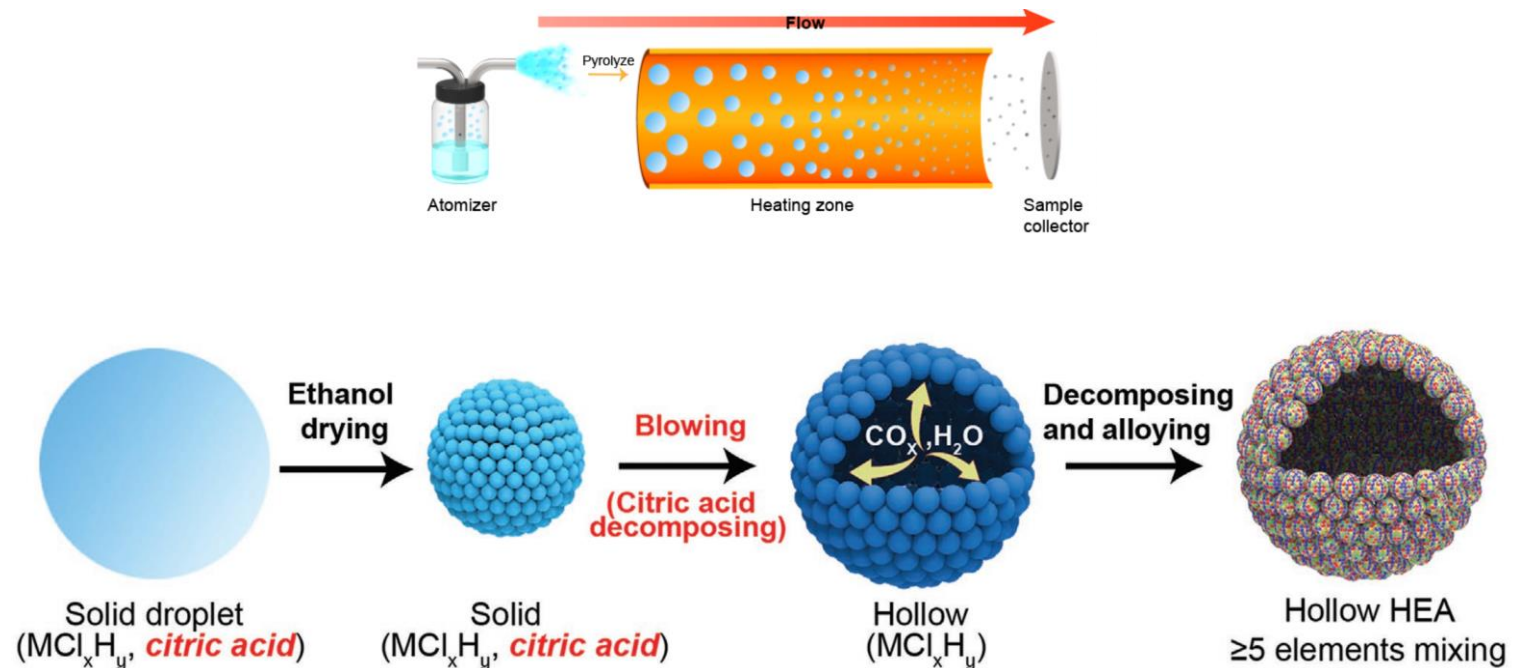
# High-Index-Facet Metal-Alloy Nanoparticles as Fuel Cell Electrocatalysts

Liliang Huang, Cindy Y. Zheng, Bo Shen, and Chad A. Mirkin\*



# Continuous Synthesis of Hollow High-Entropy Nanoparticles for Energy and Catalysis Applications

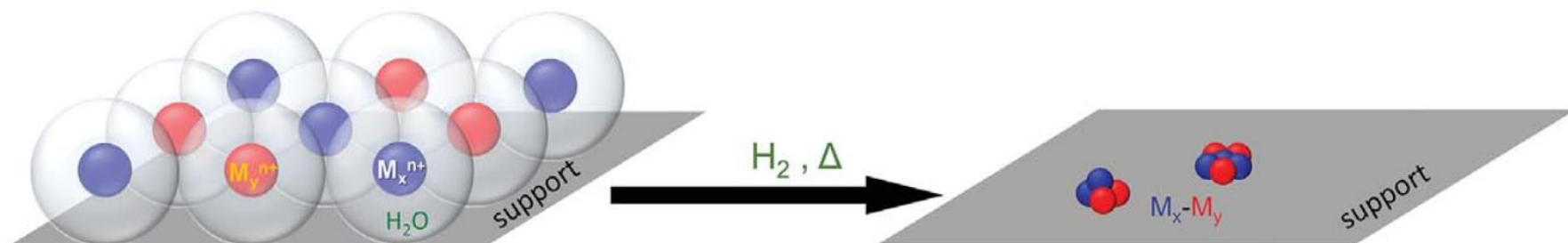
Xizheng Wang, Qi Dong, Haiyu Qiao, Zhennan Huang, Mahmoud Tamadoni Saray, Geng Zhong, Zhiwei Lin, Mingjin Cui, Alexandra Brozena, Min Hong, Qinqin Xia, Jinlong Gao, Gang Chen, Reza Shahbazian-Yassar, Dunwei Wang, and Liangbing Hu\*



# CATALYSIS

## Synthesis of ultrasmall, homogeneously alloyed, bimetallic nanoparticles on silica supports

A. Wong,<sup>1</sup> Q. Liu,<sup>1</sup> S. Griffin,<sup>1</sup> A. Nicholls,<sup>2</sup> J. R. Regalbuto<sup>1\*</sup>



## Relevance

- Electrospray – a synthetic tool
- Transformation of materials in microdroplets
- Multimetallic nanoclusters – Choice of metal systems

## Why this paper

- Novel synthetic method and mechanism
- Existing method can be tuned to achieve novelty
- Importance of the supported nanoparticles for the potential applications

## In this paper

- A general and facile fast moving bed pyrolysis (FMBP) strategy following wet impregnation for the preparation of ultrasmall and highly dispersed HEA-NPs coming up to 10 immiscible elements (Mn, Co, Ni, Cu, Rh, Pd, Sn, Ir, Pt, and Au).
- The pyrolysis of the mixed metal chlorides precursors loading on various granular supports such as carbon support (carbon black and graphene oxide),  $\gamma$ -Al<sub>2</sub>O<sub>3</sub>, and zeolite.
- In the FMBP process, the formation of HEA-NPs is thermodynamically favored due to the low free energy of the formation of nuclei, which results from the fast pyrolysis of precursors at high temperatures.
- The representative quinary (FeCoPdIrPt) HEA-NPs possess the high activity and exceptional stability toward hydrogen evolution in water splitting.



# Synthesis

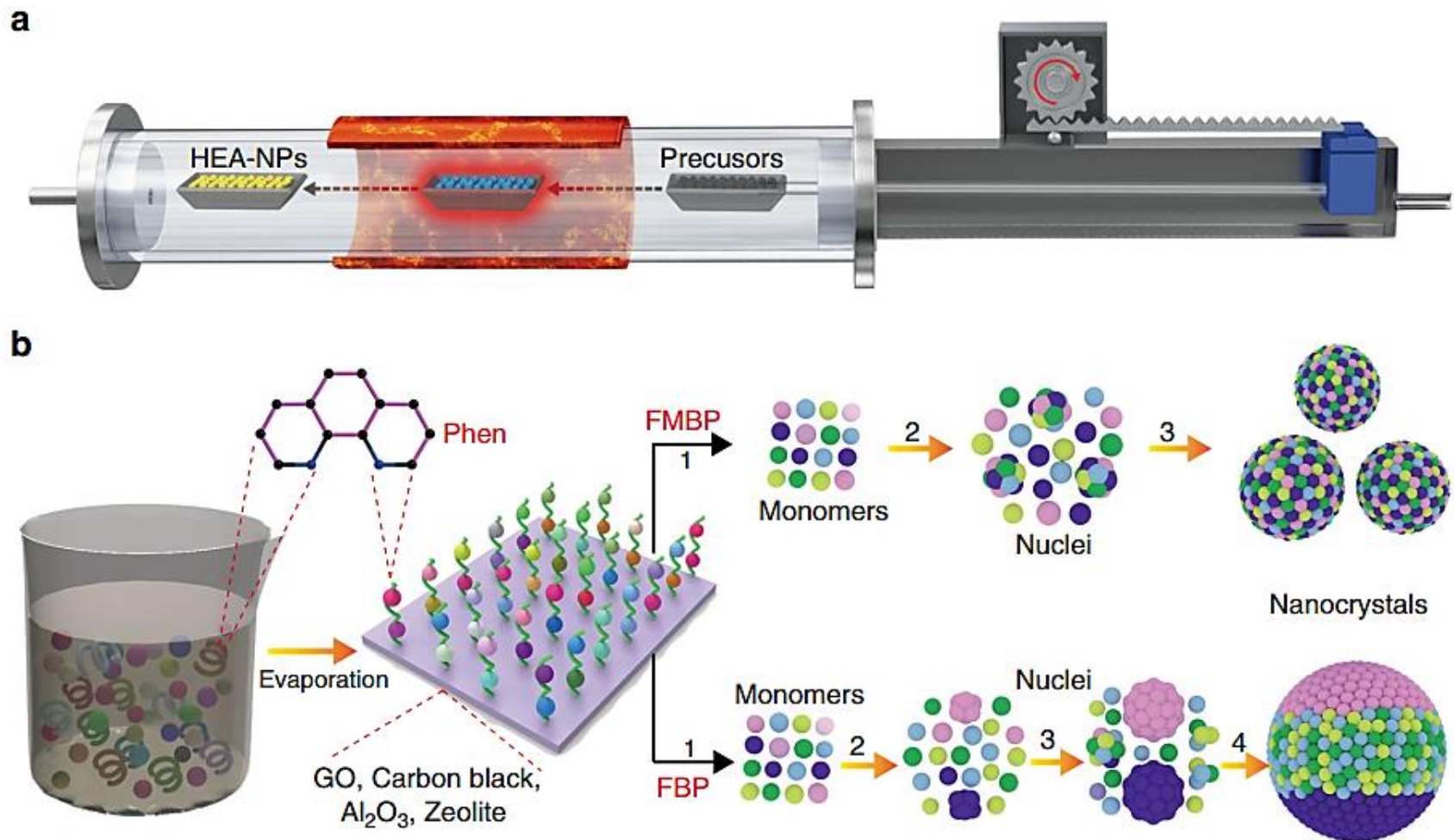
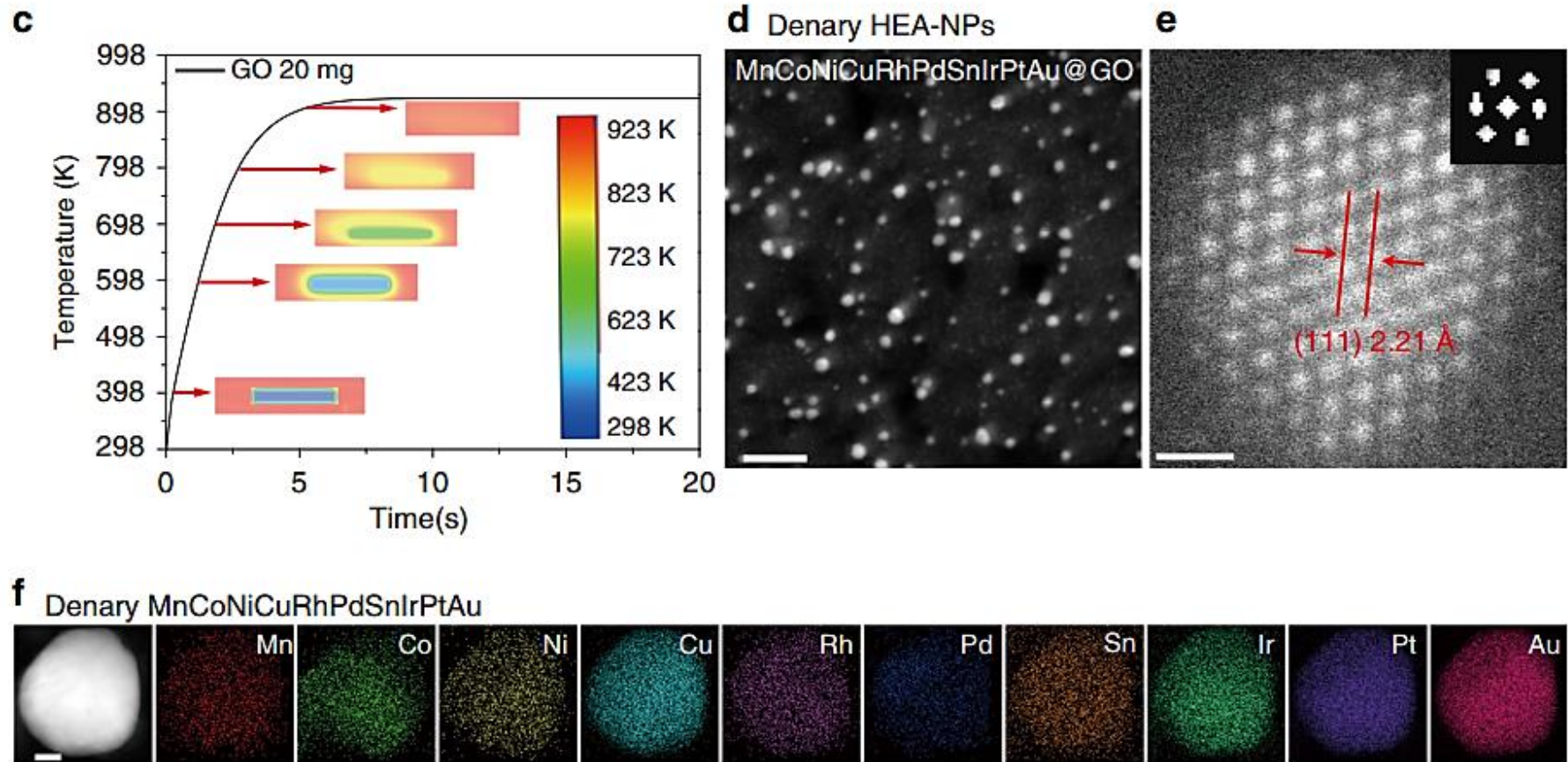


Fig: a) Schematic diagram of the FMBP experimental setup for synthesis of HEA-NPs. b) Schematic diagrams for synthesis of homogeneous and phase-separated HEA-NPs by FMBP and FBP strategies, respectively.



# Characterization



c) The simulation of the time required for precursors/GO (20 mg, 3 wt%) to reach 923 K in the FMBP process. Center: the metal precursors/GO in the quartz boat. d) HAADF-STEM images for the denary (MnCoNiCuRhPdSnIrPtAu) HEA-NPs highly dispersed on GO synthesized by the FMBP strategy (The loading of HEA-NPs on GO was 3 wt%). e) The HR-STEM image for the denary (MnCoNiCuRhPdSnIrPtAu) HEA-NPs (inset, the Fourier transform analysis for denary (MnCoNiCuRhPdSnIrPtAu) HEA-NPs indicated that the denary HEA-NPs featured with an fcc crystal framework). f) Elemental maps for denary (MnCoNiCuRhPdSnIrPtAu) HEA-NPs (The loading of HEA-NPs on GO was 10 wt%). The elements in HEA-NPs have the equal atomic ratio. Scale bar d: 10 nm, e: 0.5 nm, and f: 10 nm.

# Application of FMBP to various systems

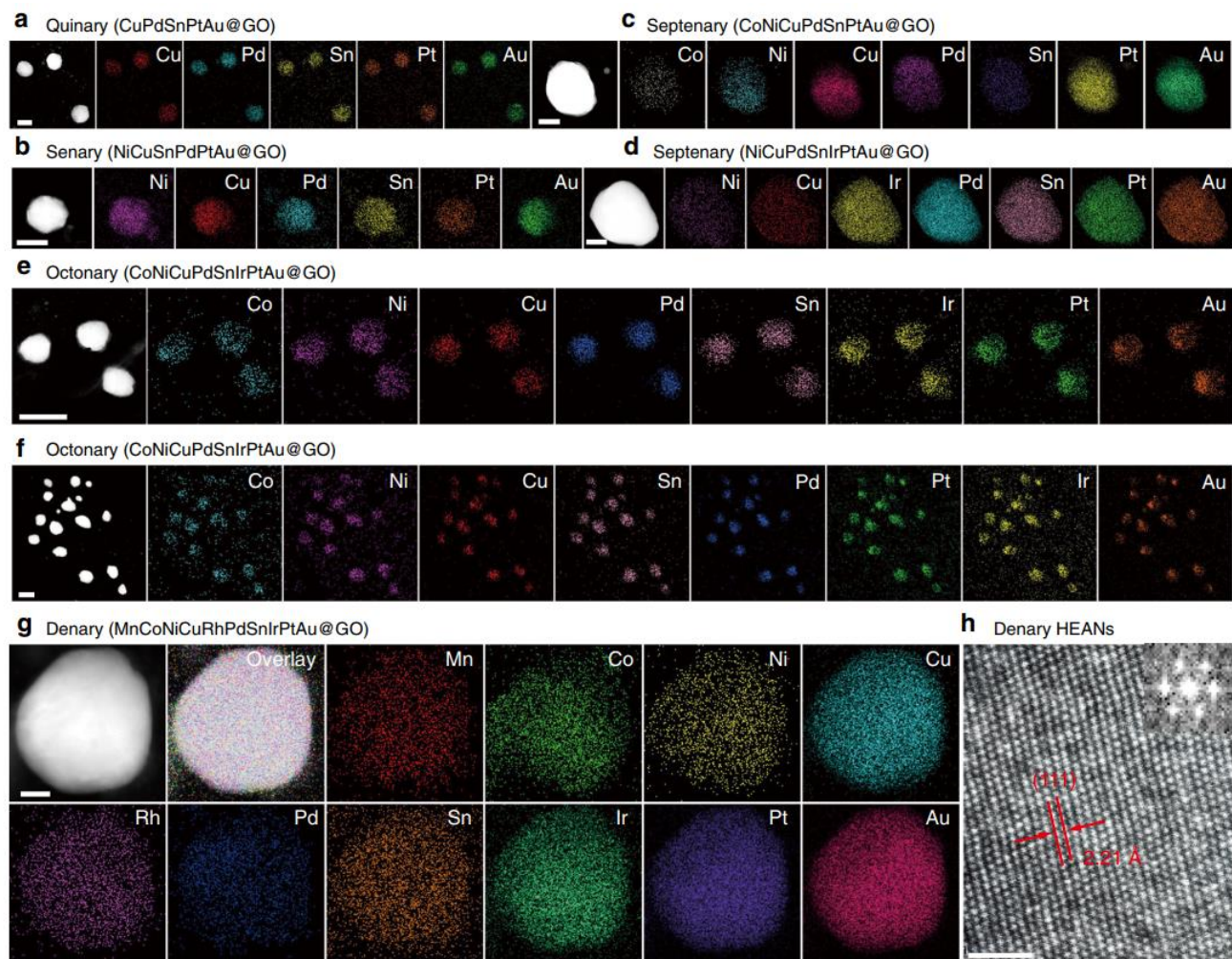


Fig. 2 HAADF and elemental maps for HEA-NPs synthesized by FMBP. HAADF and elemental maps for the quinary (CuPdSnPtAu) (a), senary (NiCuPdSnAuPt) (b), septenary (CoNiCuPdSnPtAu) (c), septenary (NiCuPdSnIrPtAu) (d), octonary (CoNiCuPdSnIrPtAu) (e) and (f), and denary (MnCoNiCuRhPdSnIrPtAu) alloy (g), and supported on GO. h The high-resolution TEM image for the denary (MnCoNiCuRhPdSnIrPtAu@GO) HEA-NPs. The inset shows the Fourier transform analysis for denary HEA-NPs indicating that the denary HEA-NPs exhibited an fcc crystal framework. The loading of HEA-NPs on GO was 10 wt%. The elements in HEA-NPs have the equal atomic ratio. Scale bar (a–c, e, f): 50 nm, d: 20 nm, g: 10 nm, and h: 1 nm.



# Characterization

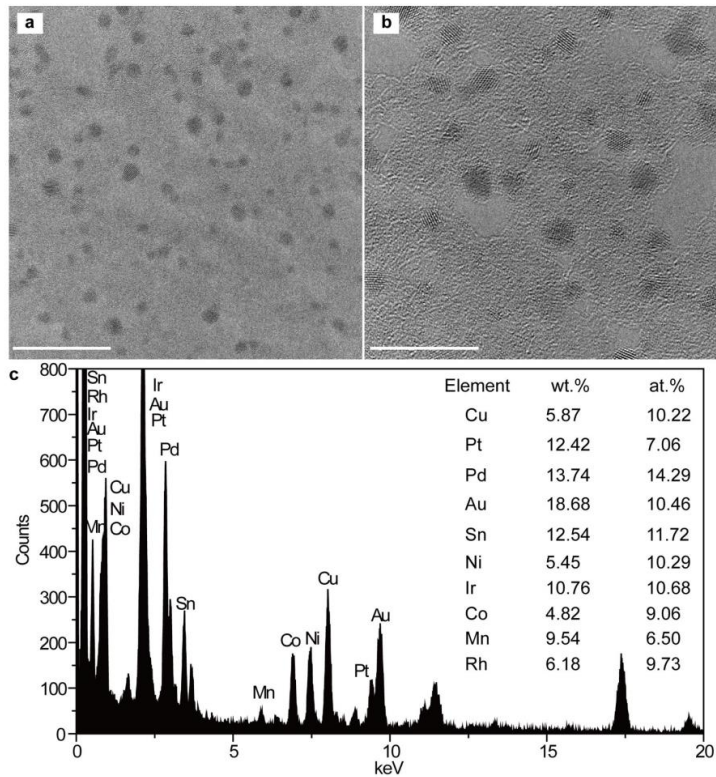


Fig: HRTEM images and EDX spectra of (MnCoNiCuRhPdSnIrPtAu) alloy. HRTEM images (a, b) and EDX spectra (c) for the denary (MnCoNiCuSnRhPdIrPtAu) HEA-NPs supported on GO at 923 K. The loading of HEA NPs on GO was 3 wt%. Scale bar a: 20 nm, b: 10 nm.

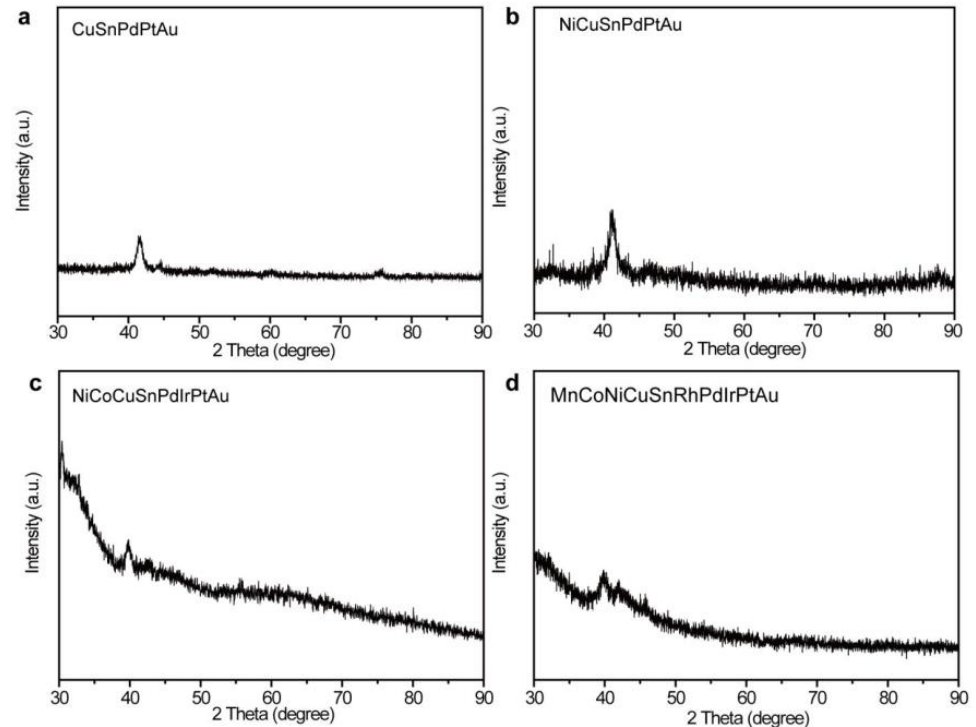


Fig: XRD patterns of alloys containing 5-10 metals by FMBP. quinary (CuSnPdPtAu) HEA-NPs (a), senary (NiCuSnPdPtAu) HEA-NPs (b), octonary (NiCoCuSnIrPdPtAu) HEA-NPs (c), and denary (MnCoCuIrNiSnRhPdPtAu) HEA-NPs (d) by FMBP at 923 K. The loading of HEA-NPs on GO was 10 wt%.

# Immobilizing HEA-NPs on various supports

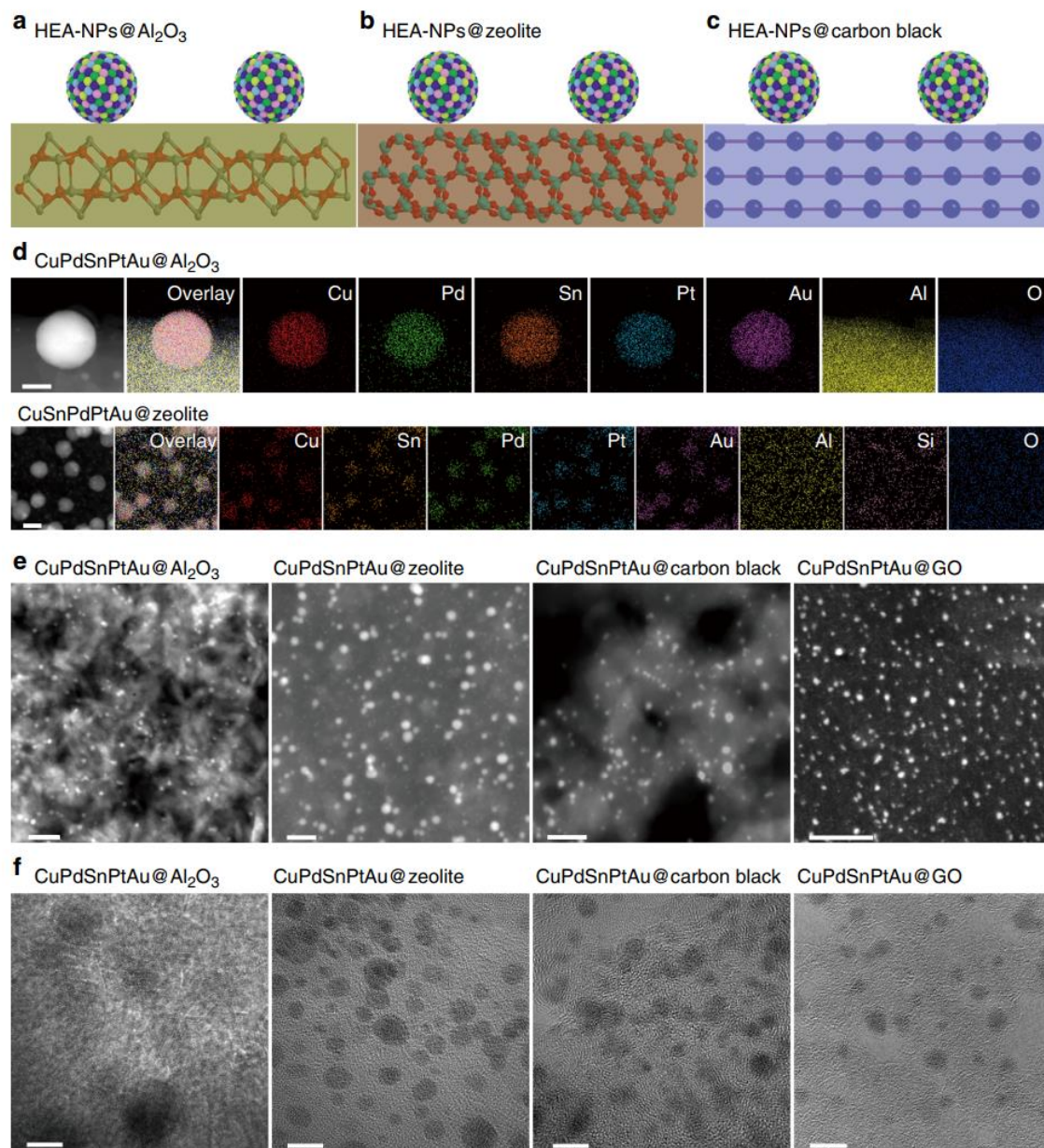


Fig. 3 Supporting HEA-NPs on various supports. The schematic diagrams for HEA-NPs dispersed on  $\gamma$ -Al<sub>2</sub>O<sub>3</sub> (a), zeolite (b), and carbon black (c). d The elemental maps for quinary (CuPdSnPtAu) supported on Al<sub>2</sub>O<sub>3</sub> and zeolite, (The loading of HEA-NPs on  $\gamma$ -Al<sub>2</sub>O<sub>3</sub> and zeolite was 10 wt%). e) STEM images revealed that the HEA-NPs synthesized by FMBP strategy were highly dispersed on  $\gamma$ -Al<sub>2</sub>O<sub>3</sub>, zeolite, carbon black, and GO. f) HR-TEM images for HEA-NPs supported on  $\gamma$ -Al<sub>2</sub>O<sub>3</sub>, zeolite, carbon black, and GO synthesized by FMBP strategy (The loading of HEA-NPs on supports was 3 wt%). The elements in HEA-NPs have the equal atomic ratio. Scale bar d: 10 nm, e: 20 nm, f: 5 nm.



# Effect of temperature on alloy formation

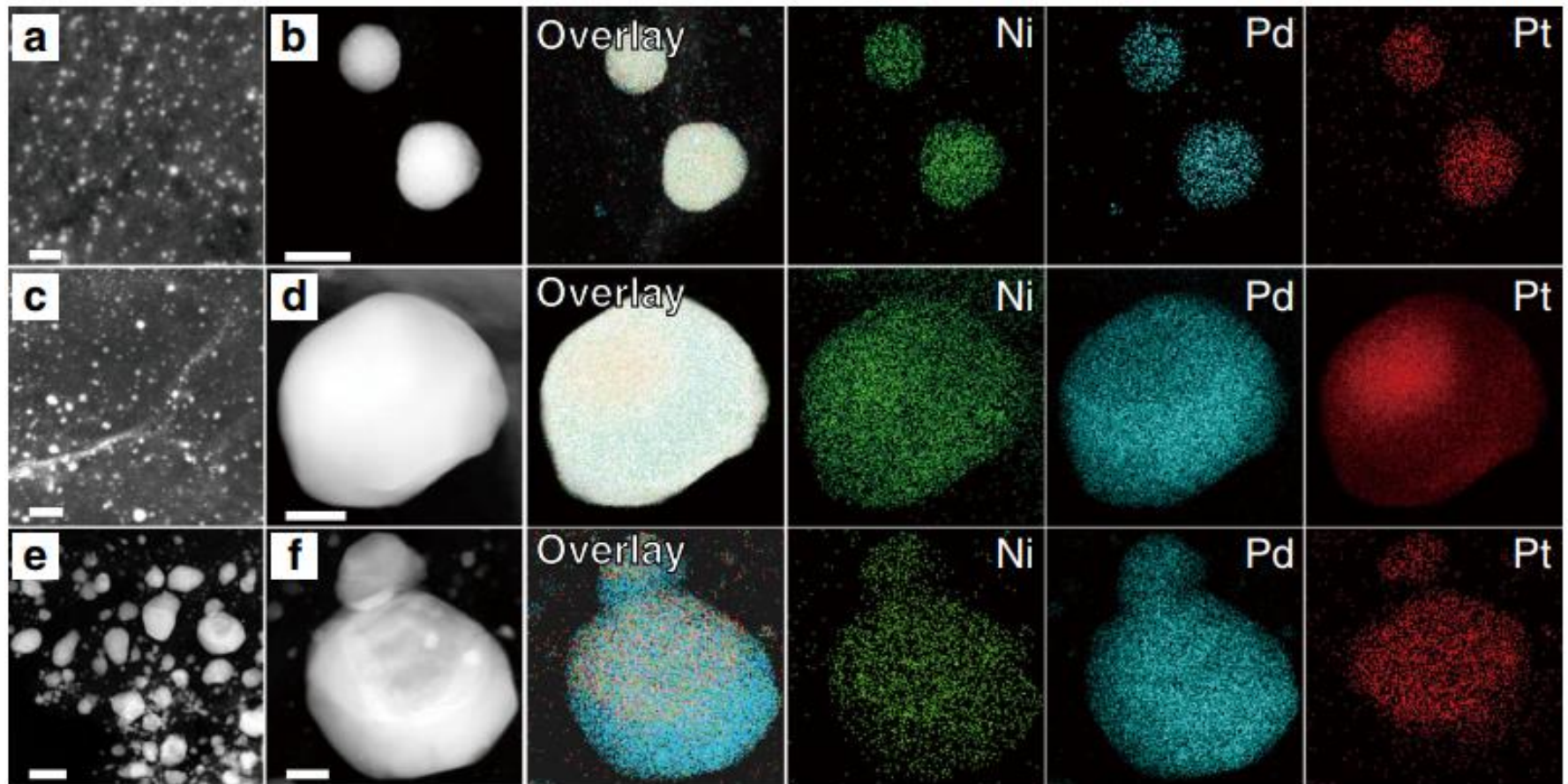


Fig. 4 Synthesis of NiPdPt by different methods. a) The STEM image of NiPdPt obtained by FMBP (923 K). b) The elemental maps of NiPdPt obtained by FMBP (923 K). c) The STEM image of NiPdPt obtained by SMBP (923 K). d) The elemental maps of NiPdPt obtained by SMBP. e) The STEM image of NiPdPt obtained by FBP. f) The elemental maps of NiPdPt obtained by FBP. The loading of HEA-NPs on GO was 3 wt% for a, c, e. The loading of HEA-NPs on GO was 10 wt% for the NiPdPt alloy for elemental maps. Scale bar a: 10 nm, (b–d, f): 50 nm, e: 200 nm.

# Control experiments

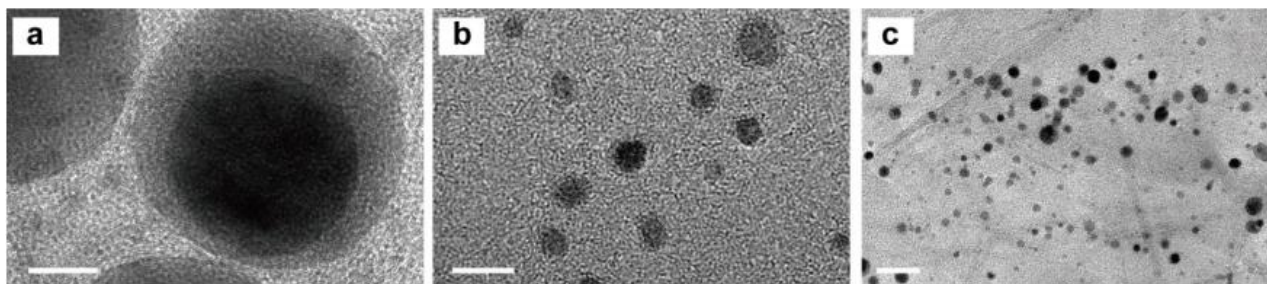


Fig: STEM images for CuSnPdPtAu by FMBP for different time. (a) 30 min, (b) 120 min, (c) 180 min. The loading of HEA-NPs on GO was 3 wt%. Scale bar (a-b): 10 nm, c: 20 nm.

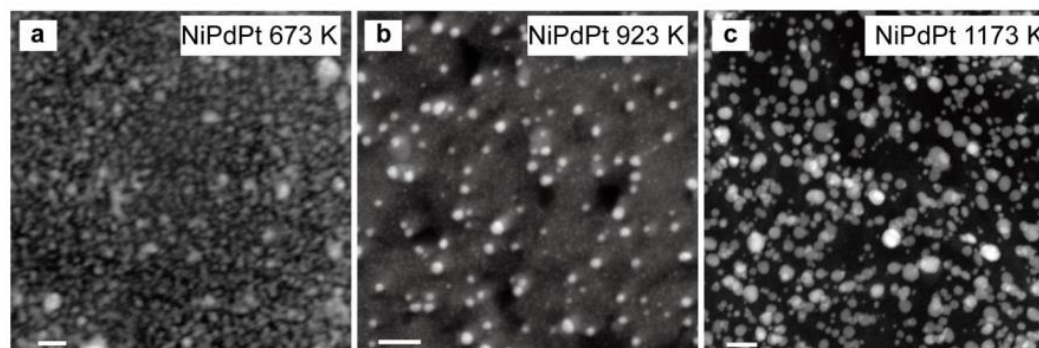
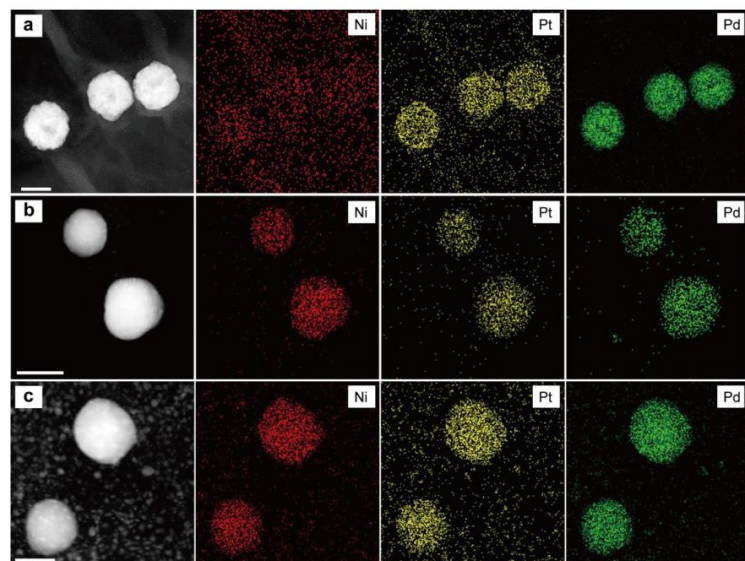
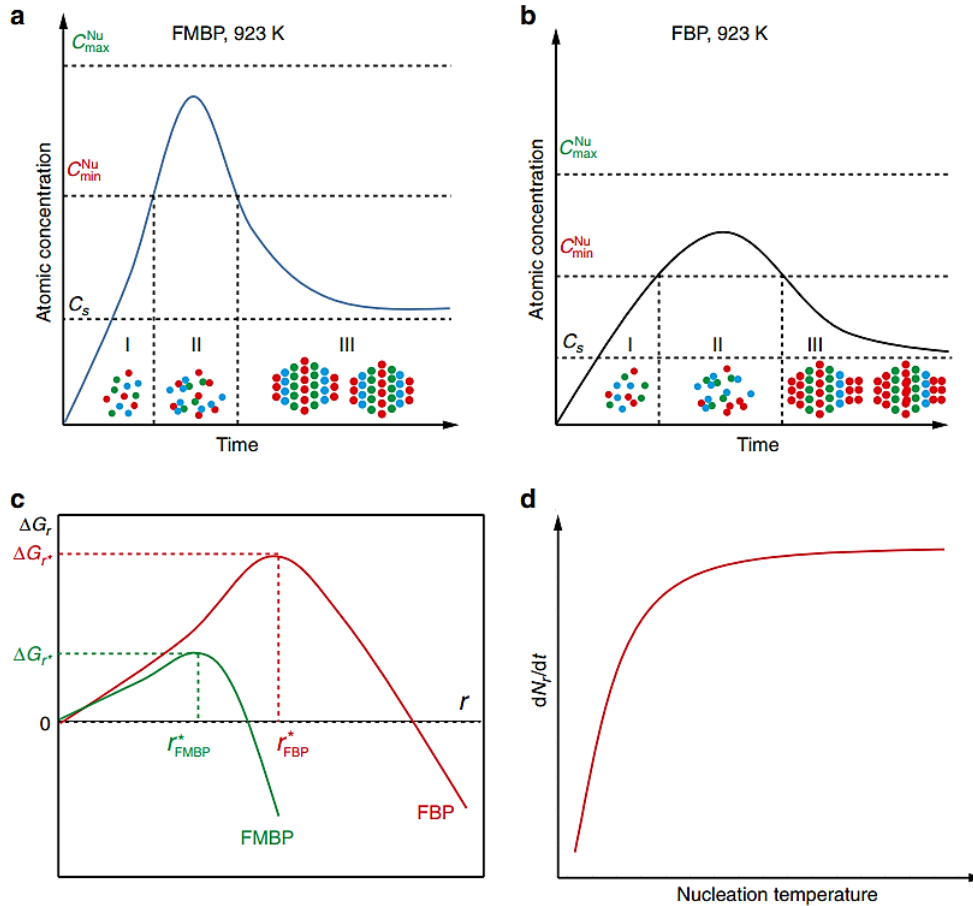


Fig: STEM images for NiPdPt by FMBP at different temperature. The ternary (NiPdPt) alloy supported on GO synthesized by the FMBP method at 673 K (a), 923 K (b), and 1173 K (c), respectively. The loading of HEA-NPs on GO was 3 wt%. Scale bar (a-b): 10 nm, c: 20 nm.

Fig: Elemental maps of NiPdPt by FMBP at different temperature. The ternary (NiPdPt) alloy supported on GO synthesized by the FMBP method at 673 K (a), 923 K (b), and 1173 K (c), respectively. The loading of HEA-NPs on GO was 10 wt%. Scale bar (a-b): 50 nm, c: 70 nm.

# Mechanism of formation of HEA-NPs



$$\Delta G_r = 4\pi r^2 \gamma + \frac{4}{3} \pi r^3 \Delta G_V \quad (1)$$

$$\Delta G_V = -\frac{RT \ln S}{V_m} \quad (2)$$

$$\Delta G_r = 4\pi r^2 \gamma + \frac{4}{3} \pi r^3 \Delta G_V = 4\pi r^2 \gamma - \frac{4}{3} \pi r^3 \frac{RT \ln S}{V_m} \quad (3)$$

$$r^* = \frac{2\gamma V_m}{RT \ln S} \quad (4)$$

$$\Delta G_{r^*} = 4\pi r^{*2} \gamma - \frac{4}{3} \pi r^{*3} \frac{RT \ln S}{V_m} \quad (5)$$

Fig. 5 Mechanism of formation of nanocrystals by FMBP and FBP. a The diagrams of formation of monomers (I), nucleation (II), and growth of nanocrystal (III) versus the reaction time by FMBP. b The diagrams of formation of monomers (I), nucleation (II), and growth of nanocrystal (III) phases versus the reaction time by FBP. c) The corresponding overall free energy change ( $\Delta G_r$ ) versus the nucleus size ( $r$ ) via FMBP, and FBP strategies. d The effect of nucleation temperature on the nucleation rate ( $dN_r/dt$ ).



# HER tests

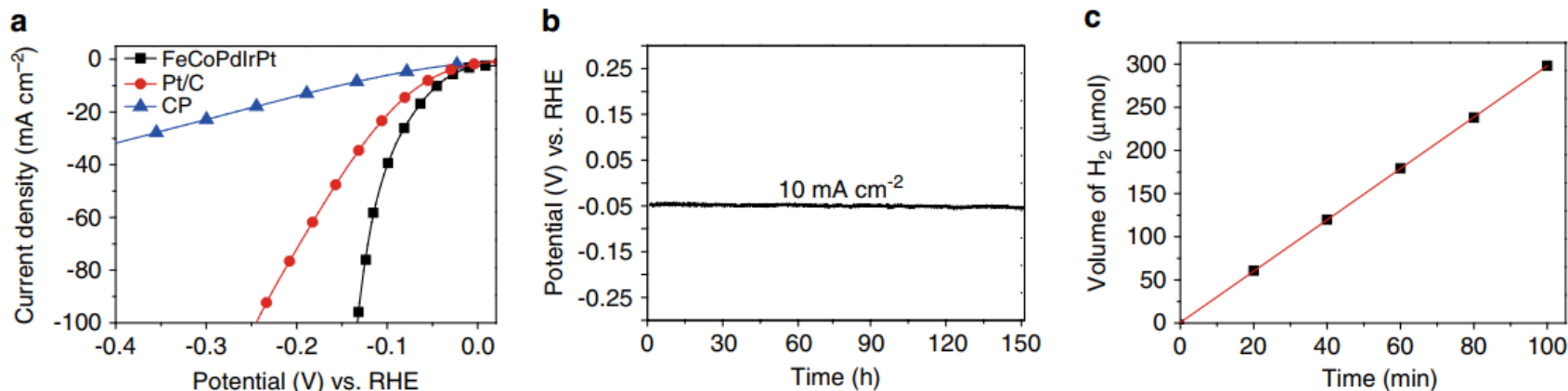


Fig: Electrochemical HER performance of samples. a) The activities toward HER of the prepared FeCoPdPtIr@GO and Pt/C, and pure CP eOur FMBP strategy allows electrodes. Linear sweep voltammetry (LSV) curves were conducted to evaluate the activity toward HER at a scan rate of  $5 \text{ mV s}^{-1}$  with iR correction. The mass loading of HEA-NPs on GO was 3 wt%. b) Chronopotentiometry curve for FeCoPdIrPt@GO. c) The amount of  $\text{H}_2$  during HER.

# Summary

- A facile synthesis strategy, i.e. fast moving bed pyrolysis, for synthesizing the ultrasmall homogeneous HEA-NPs with up to ten elements (MnCoNiCuRhPdSnIrPtAu) highly dispersed on various granular supports.
- This strategy ensures the mixed metal precursors to be simultaneously pyrolyzed at high temperatures, which results in the high supersaturation of monomers and the small size of nuclei, producing the highly dispersed HEA-NPs on supports.
- The parameters and mechanism of fast moving bed pyrolysis for producing HEA-NPs are investigated.
- The representative FeCoPdIrPt HEA-NPs exhibit the smaller overpotential and the higher mass activity of HER in electrochemical water splitting as compared with the commercial Pt/C.